

Interferometry and spectroscopy of β Cen: a β Cephei star in a binary system^{*}

J. G. Robertson,^{1†} T. R. Bedding,¹ C. Aerts^{2‡}, C. Waelkens², R. G. Marson^{1,3} and J. R. Barton⁴

¹*School of Physics, University of Sydney 2006, Australia*

²*Instituut voor Sterrenkunde, Celestijnenlaan 200 B, B-3001 Leuven, Belgium*

³*Current address: NRAO Array Operations Center, P.O. Box 0, Socorro NM 87801, USA*

⁴*Anglo-Australian Observatory, P.O. Box 296, Epping 2121, Australia*

2 December 2024

ABSTRACT

β Cen is a bright β Cephei variable and has long been suspected to be a binary. Here we report interferometric observations with the 3.9-m Anglo-Australian Telescope at a single epoch which show the star to be a binary with components separated by 15 milliarcsec and having approximately equal luminosities at 486 nm. We also present high-resolution spectra taken over five nights with the ESO CAT which show β Cen to be a double-lined spectroscopic binary. We identify two pulsation frequencies in the primary. Further spectroscopic and interferometric studies of this double star should allow determination of its orbital parameters and component masses.

Key words: stars: individual: β Cen – stars: variables: other – techniques: interferometry

1 INTRODUCTION

β Cen (HR 5267) is a bright early-type southern star. It has been of interest to observers as a β Cephei variable, as a probe of the intervening interstellar medium, and also as a stellar X-ray source. β Cen was observed by the Narrabri Stellar Intensity Interferometer in 1963 as a target for commissioning observations of that instrument (Hanbury Brown 1974). The maximum correlation observed was, however, only half the expected value. This could be explained if β Cen were a double star with components of similar brightness. The Intensity Interferometer results could not directly demonstrate the binarity of β Cen, nor determine the separation, because the angular separation was resolved by the individual 6.5 m reflectors. But a value greater than about a few hundredths of an arcsecond would be expected. The alternative explanation of a single star surrounded by a halo was considered unlikely since no narrow emission or absorption lines were seen in the spectrum (Shobbrook & Robertson 1968).

Binarity was also suspected by Breger (1967) and Shob-

brook & Robertson (1968) from radial velocity measurements. The latter authors were seeking to clarify the low correlation found by the Intensity Interferometer. They found velocity variations with a short period (0.135 d), indicative of a β Cephei variable, and a long period (352 d), ascribed to orbital motion in a binary system. A more comprehensive spectroscopic analysis was made by Lomb (1975), who classed the star as a single-lined spectroscopic binary and gave the short period as 0.157 d.

Here we report further observations of β Cen, both interferometric and spectroscopic, which conclusively demonstrate binarity. We have also identified two pulsation frequencies in the primary from radial-velocity variability. Further observations will be needed to find the parameters of the orbit.

2 INTERFEROMETRIC MEASUREMENTS

2.1 Observations

We have carried out observations of β Cen using aperture masking, which involves modifying the telescope pupil with a mask (Haniff et al. 1987). Our aperture masks contain a small number of non-redundantly spaced holes, each of size comparable to or smaller than the Fried length r_0 . Compared

^{*} Based on observations obtained at the Anglo-Australian Observatory and the European Southern Observatory, Chile

[†] E-mail: jgr@physics.usyd.edu.au

[‡] Postdoctoral Fellow, Fund for Scientific Research, Flanders (Belgium)

Table 1. Journal of MAPPIT observations of β Cen

Date (UT)	$\lambda/\Delta\lambda$ (nm)	Mask pattern	Longest baseline* (m)	Hole size* (cm)	Detector field (arcsec)	Observed position angles (North through East) (degrees)	Seeing (arcsec)
1995/1/12	650/40	A	3.28	4.7	3.3 x 5.8	87.8, -31.1, 29.8	1.1
1995/1/12	650/40	B	3.67	4.7	3.3 x 5.8	5.1, 60.2, 11.1, -57.8	1.2
1995/1/14	486/10	B	3.67	7.9	2.3 x 4.1	-1.1, -90.0, -89.4, 45.9, -42.8, 4.2, -60.3, 74.8, -13.5, 33.6, 82.2, -3.0, -71.9, -71.3	~ 1 (cloud-affected)

*As projected on primary mirror

with a fully-filled aperture, as used in speckle interferometry, such observations provide better calibrated measurements and reach the full diffraction limit. This comes at the expense of a brighter limiting magnitude and less complete spatial-frequency coverage, neither of which is important for a bright double star. As we show in this paper, the Non-Redundant Masking (NRM) method gives very clear resolution of a binary at 15 mas from observations with a 4 m-class telescope, whereas speckle interferometry with similar telescopes is limited to separations of greater than 30 mas (McAlister 1997).

We observed β Cen in 1995 January with the MAPPIT interferometer (Masked APerture-Plane Interference Telescope; Bedding et al. 1994), which is situated at the coude focus of the 3.9-m Anglo-Australian Telescope (AAT). The instrumental setup was the same as that described by Bedding et al. (1997). Table 1 gives particulars of the observations. The unresolved star α^1 Cen was observed with each of the three wavelength/mask combinations tabulated, to provide calibration of the fringe visibility loss due to residual atmospheric effects. A Dove prism was used as a field rotator to obtain a range of observed position angles, and an atmospheric dispersion corrector was used during all observations. The binary stars ADS 7846, ADS 7982, ADS 8573 and γ Vir were observed to provide a calibration of the spatial scale and position angle.

Two different aperture masks were used, both having 5 square holes in a straight line and giving 10 simultaneous non-redundant baselines. The mask layouts are shown in Fig. 1 (only one mask was used at a time). Design A gives a nearly uniform spacing of the baselines (Marson 1994), but is limited to a maximum baseline of 3.28 m by the need to fit the holes around the central obstruction of the telescope. The other design has a maximum baseline of 3.67 m, close to the largest that can reliably be fitted on the AAT primary mirror, but accepts a non-uniform distribution of baselines (Bedding 1992). For the present observations, where the visibility as a function of baseline is expected to take the simple form given by a binary star, both masks are suitable. The longer baseline mask and shorter wavelength were used in later runs to help ensure that we observed the null of the binary visibility curve.

The detector was a Thomson CCD, with a window of 230 columns by 400 rows. The CCD was used in time series mode with full column binning (e.g., Buscher et al. 1990), giving a 230×1 readout every 13 ms. In this mode it was pos-

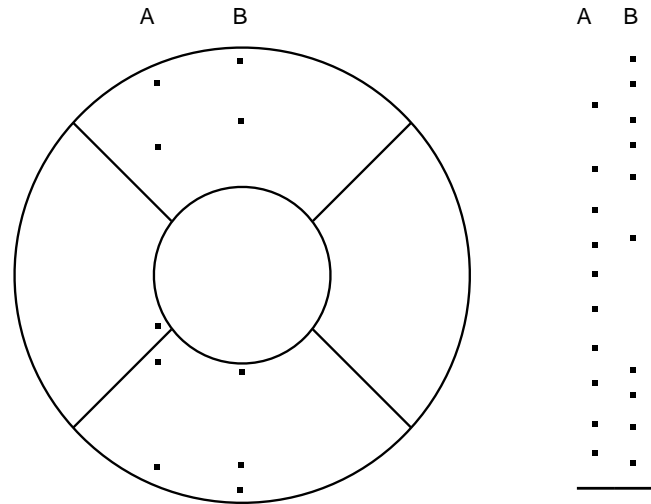


Figure 1. Non-redundant mask designs for MAPPIT, with the pupil of the AAT drawn to the same scale. The five holes in array A have relative positions (scaled to the longest baseline) of 0, 0.275, 0.367, 0.833 and 1.000. The holes in array B are at relative positions 0, 0.058, 0.275, 0.858 and 1.000. The columns on the right show the spatial frequency coverage of the two arrays (the line at the bottom is the origin). The holes as shown have sizes, as projected on the primary mirror, of 4.7 cm.

sible to observe using a 100% duty cycle, i.e., with the shutter open continuously during each 130-s run. Full column binning was possible without smearing the fringes because the fringes were arranged to lie accurately along columns.

2.2 Data analysis

The interferometric data consisted of 21 runs spaced over the full range of position angles (see Table 1), and with 10 baselines for every run. Power spectra were computed for each of the 10,000 exposures in a run, and then combined to give an average power spectrum for that run. The average power spectra exhibited 10 peaks, from the 10 non-redundant baselines. The heights of these peaks were measured in order to find the observed values of V^2 (the square of the fringe visibility). These were calibrated by dividing by the corresponding values from the observation of the calibration star. An advantage of NRM is that the peak heights can be measured relative to their local background, thereby allowing for noise variance contributions to the power spectra.

The individual stellar discs of hot stars cannot be resolved by baselines limited to 4 m. β Cen (spectral type B2)

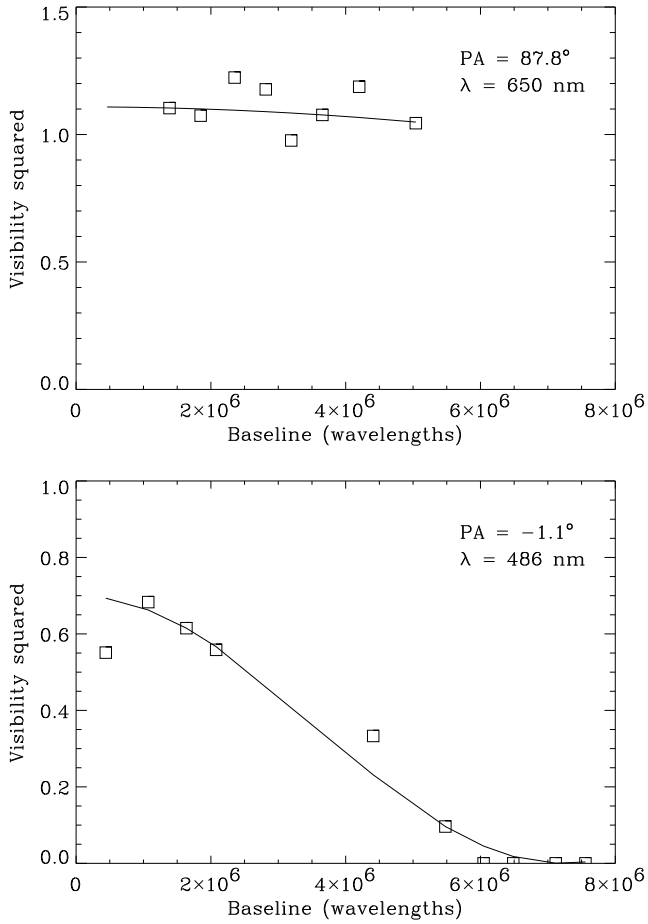


Figure 2. Two examples of V^2 fits for MAPPIT observations of β Cen. The symbols show measured values and the curves are two-parameter fits, as described in the text.

thus falls in the class of binary stars with the individual stellar discs unresolved, for which V^2 is given by

$$V^2 = \frac{1}{(1 + \beta)^2} [\beta^2 + 1 + 2\beta \cos \{(2\pi\theta d \cos \psi)/\lambda\}], \quad (1)$$

where β is the brightness ratio of the two components, θ is their angular separation, ψ is the angle on the plane of the sky between the line joining the two components and the projection of the interferometer baseline, λ is the observing wavelength and d is the interferometer baseline length (Hanbury Brown et al. 1967).

We have adopted a two-step process in fitting the functional form expected for a binary star to the data. The first step consisted of the separate treatment of each calibrated run. Figure 2 shows two examples, with different degrees of visibility taper due to the different angles ψ . Runs with ψ near 0, i.e., those that best resolve the double, show that V^2 does exhibit nulls. This indicates that the two stars have equal brightness to within the observational accuracy (the limit which can be placed on the magnitude difference is discussed below). The model fit to each run was therefore specialised to the case of $\beta = 1$, giving

$$V^2 = \frac{1}{2} [1 + \cos \{(2\pi\theta d \cos \psi)/\lambda\}]. \quad (2)$$

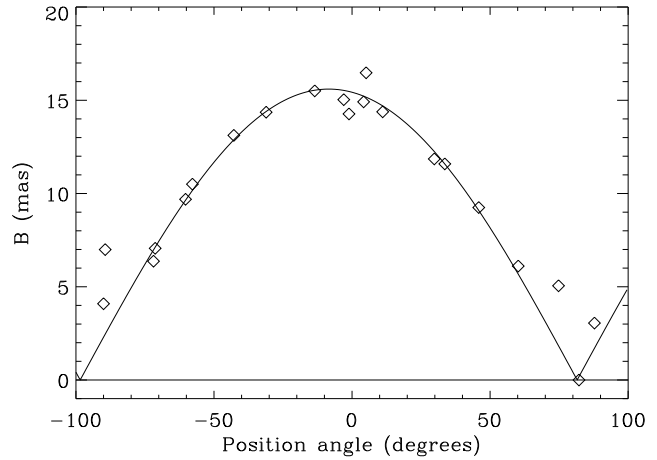


Figure 3. Projected angular separation of β Cen as a function of position angle. Each symbol is the result of a fit to observations at a single position angle. The curve shows the best-fit theoretical model for a binary star with components of equal luminosity.

For each run, two free parameters A and B were allowed, by fitting the following model functional form to the observed values of V^2 :

$$V_{\text{mod}}^2 = \frac{1}{2} A [1 + \cos (B 2\pi d/\lambda)]. \quad (3)$$

The parameter B depends on the degree of taper of the visibilities with baseline (large B values indicate strong taper), which in turn depends on the position angle difference, ψ . Ideally, the parameter A should be 1.0 for calibrated observations. In practice, it was clear that the internal consistency of the visibilities for the 10 baselines within each run was better than the consistency between runs, and it was preferable to allow the overall visibility normalisation of each run to float by fitting the A values. Variations in atmospheric conditions between calibrator and target star, including the effects of cloud on some runs, were probably responsible.

The fitting process for each run consisted of finding the values of A and B which minimised the value of the sum over the data points of

$$\left| \frac{V_{\text{obs}}^2 - V_{\text{mod}}^2}{V_{\text{mod}}^2 + 0.2} \right|, \quad (4)$$

where V_{obs} refers to the observed visibilities. Minimum absolute value rather than a least squares fit was used to obtain a more robust treatment of the non-Gaussian errors, which arise from residual atmospheric effects on the values of V^2 . The reason for minimising the expression as shown is to allow for the observed greater absolute errors at high visibilities, giving a process intermediate between the assumptions of constant absolute errors and constant fractional errors. With the additive constant 0.2 in the denominator, a deviation between model and data at $V^2 \sim 1$ can be 6 times the deviation at low visibilities ($V^2 \sim 0$) for the same contribution to the sum of misfit terms and hence equal influence on the fitting function.

The second step in the data reduction was to make a fit to the 21 values of the parameter B as a function of the

observed position angle. Figure 3 shows the result. Breaking the fitting process into two steps in this way enables the data quality to be clearly illustrated, because Figure 3 shows 21 independent data points, fitted by a model which depends on only two parameters. Note that B is the angular separation of the stars as projected along the interferometer baseline. Consistent with Equation (2), the model functional form we have fitted is

$$B = |\theta \cos(\phi_{\text{obs}} - \phi)|, \quad (5)$$

where ϕ_{obs} is the position angle on the sky at which observations are made and ϕ is the position angle of the line joining the two stars. The parameters to be fitted are the separation θ and the true sky position angle ϕ . The observed position angles have been folded into the range $-90^\circ < \phi_{\text{obs}} \leq 90^\circ$. In principle, closure phases could be derived from the data and used to resolve the 180° ambiguity, but this is not feasible for the present case in which the component stars are nearly equal in brightness.

2.3 Results

The results in Fig. 3 show clearly that the parameter B follows the expected functional form. The points with low B values have larger uncertainties, principally because the available maximum baseline does not then reach the visibility null or close to it. For this reason, robust fitting was again achieved by minimising the sum of absolute values of the deviations between the model and data, as seen in Fig. 3.

We obtain an angular separation between the two components of 15.6 ± 2 mas and a sky position angle of $-8.5^\circ \pm 6^\circ$ (with a 180° ambiguity). The uncertainties allow for the scatter as shown in Fig. 3 (at 1σ level), and additional systematic errors in the angular scale and position angle calibration. Measuring position angle from North through East, our final values for separation and position angle are therefore 15.6 ± 2 mas and either $352^\circ \pm 6^\circ$ or $172^\circ \pm 6^\circ$.

Equation (1) shows that the two components must have equal brightness in order for the visibility versus baseline curve to have a null. Our data do show nulls where the observed position angle is appropriate, and thus our results are consistent with two stars of exactly equal magnitude. To set a limit on the magnitude difference, we have examined the regions of the nulls and find a limit of $V^2 < 0.015$ ($\sim 2\sigma$), which corresponds to a magnitude difference $\Delta m < 0.3$ (at 486 nm).

Another limit to the magnitude difference can be obtained from the Intensity Interferometer observations by Hanbury Brown et al. (1974). The ‘zero-baseline correlation’ for β Cen was found to be 0.47 ± 0.02 . The minimum value predicted by theory for a binary system with unresolved individual components is 0.5, which occurs for components of equal brightness. The observed value implies equal components, and with the given uncertainty corresponds to a limit $\Delta m < 0.3$ (2σ , at 461 nm), consistent with our result.

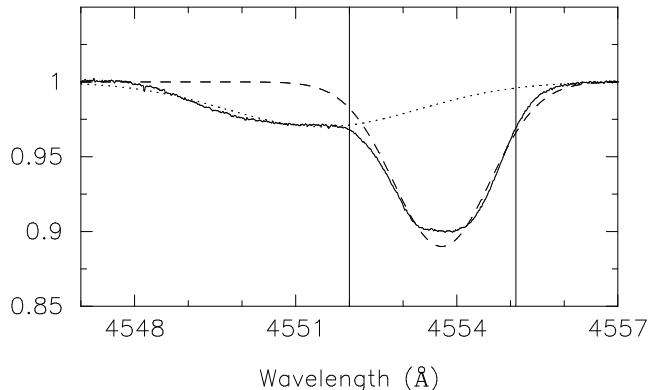


Figure 4. The average profile of the $\lambda 4553$ Å Si III line of our β Cen data set of 1988 May (full line). The dashed and dotted lines show the best Gaussian fits for the primary and secondary respectively. The vertical lines denote the integration limits for calculation of the first velocity moments of the primary’s line.

3 SPECTROSCOPIC OBSERVATIONS

In the course of a systematic study of line-profile variations in β Cep stars started in the 1980s (Aerts 1993), we have obtained 50 high-resolution ($R = 100\,000$), high S/N (> 300) spectra of β Cen taken during five consecutive nights (1988 May 16-20). The observations were performed at the European Southern Observatory in Chile with the CAT/CES instrumentation using a Reticon detector. We observed the Si III line at $\lambda 4553$ Å. Integration times were typically 5 minutes, which is less than 1% of the pulsation period of 0.157 days (6.37 cycles/day, hereafter abbreviated as c/d) proposed for β Cen by Lomb (1975). The wavelengths and radial velocities we give are heliocentric.

3.1 Average line profiles

The average profile of the 4553 Å Si III line is shown in Fig. 4 and clearly reveals β Cen to be a double-lined spectroscopic binary. For convenience we will refer to the star producing the stronger and narrower line, with clear β Cep line profile variations (see Section 3.2), as the primary, and the other as the secondary, despite their essentially equal magnitudes. The secondary has a broader line, presumably due to faster rotation.

We have determined the best Gaussian fit to the average line profiles of the primary and of the secondary component (shown as dashed and dotted lines in Fig. 4). We derive upper limits for the projected rotation velocities of $v \sin i = 120$ km s $^{-1}$ and 265 km s $^{-1}$ for the primary and secondary, respectively. More accurate values cannot be derived, since it is unclear from our data what fraction of the broadening of the lines is due to pulsation. It should be mentioned that all radial velocity values listed in the literature so far are based on the assumption of a single-lined spectroscopic binary and must therefore be treated with caution.

The two-component fit to the average spectra also yields equivalent widths of 250 ± 10 mÅ and 140 ± 10 mÅ, respectively. The tables by Becker & Butler (1990) list non-LTE

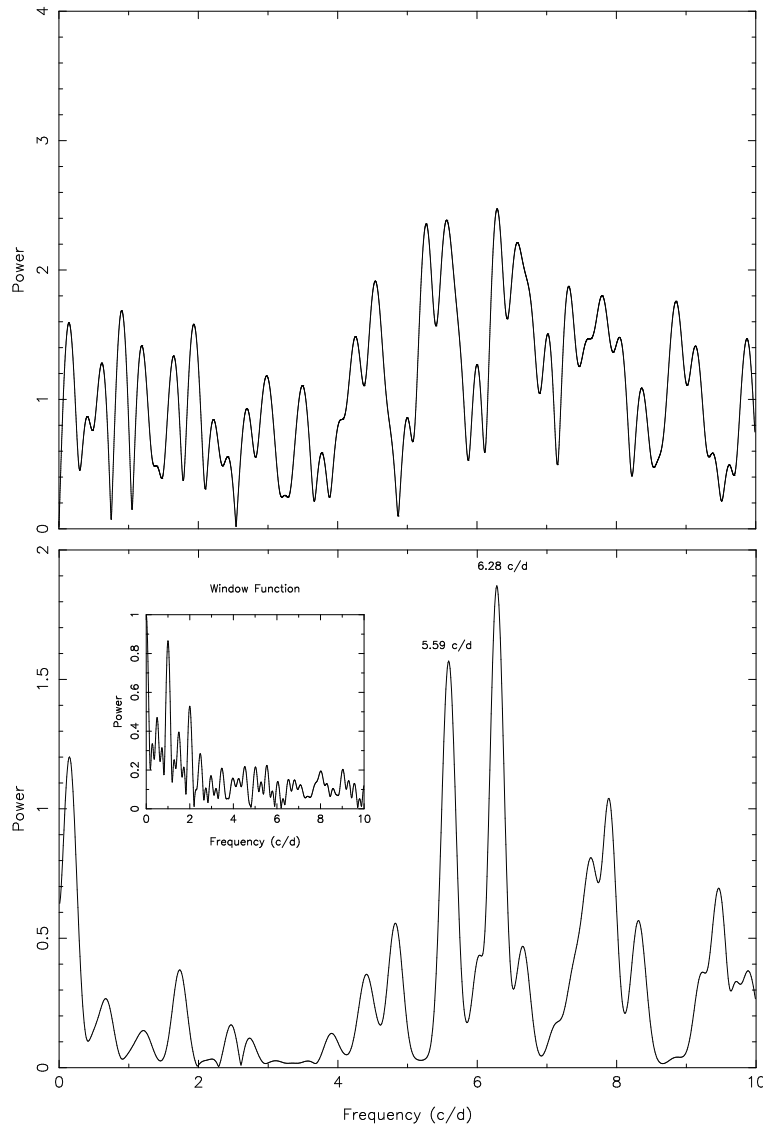


Figure 5. Power spectrum of radial velocity measurements of β Cen. The upper panel shows the raw power spectrum and the lower panel shows the results after CLEANing. The inset shows the power spectrum of the window function.

equivalent widths for Si II, III, and IV as a function of temperature, gravity, abundance, and turbulent velocity. Considering all possible ranges for the abundance and the turbulent velocity for the two components, and allowing for the equivalent width uncertainties, these tables give the following ranges for T_{eff} and $\log g$, respectively: 21 000–25 000 K and 3.1–4.5 for the primary and 19 000–21 000 K and 3.3–4.5 for the secondary. These temperature and gravity estimates agree with the values derived from Strömgren photometric data, assuming a single star (e.g., Shobbrook 1985). Our temperature estimate for the secondary argues against Shobbrook & Robertson’s (1968) suggestion that the companion is hotter than the primary. Furthermore, the temperature difference between the two stars is consistent with zero, and is therefore also consistent with the limits on the magnitude difference found from our interferometric observations.

3.2 Line-profile variations

Our spectra show clear indications of line-profile variability. While the temporal coverage is limited (50 spectra over five consecutive nights), it is more complete than previous studies (see below). This encouraged us to undertake a period search in our data. The line profiles in individual spectra are asymmetric, making them unsuitable for Gaussian fitting, so we have chosen instead to calculate the first velocity moment. We did this for the stronger line using the procedure given by (e.g., Aerts et al. 1992) and the integration limits shown in Fig. 4. Analysis of the weaker line is discussed below.

The upper panel of Fig. 5 shows the power spectrum of the velocity measurements. There is an excess of power centred at 6 c/d, with the two strongest peaks being at 5.6 and 6.3 c/d. With each of these are associated sidelobes at ± 1 c/d, which we have removed using the CLEAN algorithm (Roberts et al. 1987). The result is shown in the lower

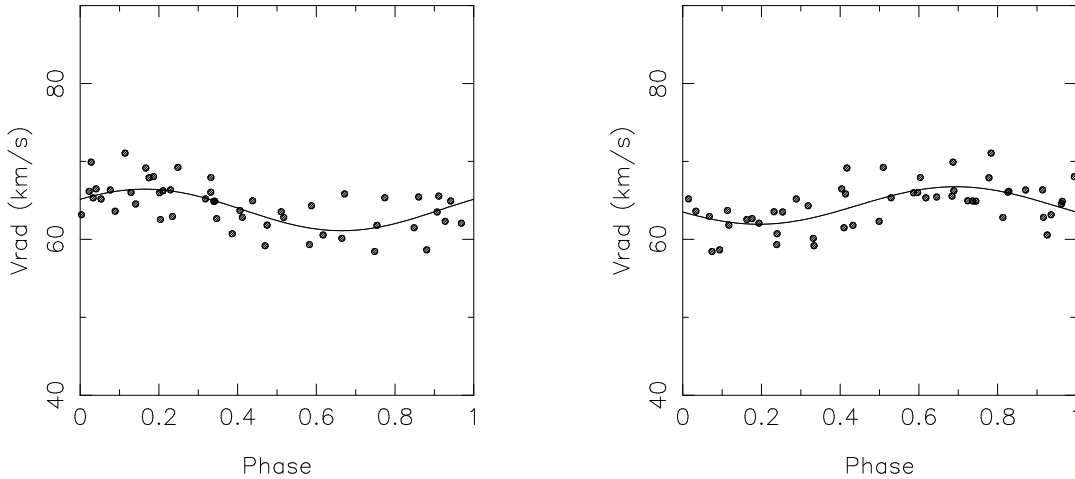


Figure 6. Radial-velocity curves measured from the stronger spectral line, phased to the frequencies $f_1 = 5.59$ c/d (left) and $f_2 = 6.28$ c/d (right). The dots represent the data, while the full line is the fit. We have used the same scale as Shobbrook & Robertson (1968) and Lomb (1975) in order to be able to compare the scatter in the diagrams with previously suggested models.

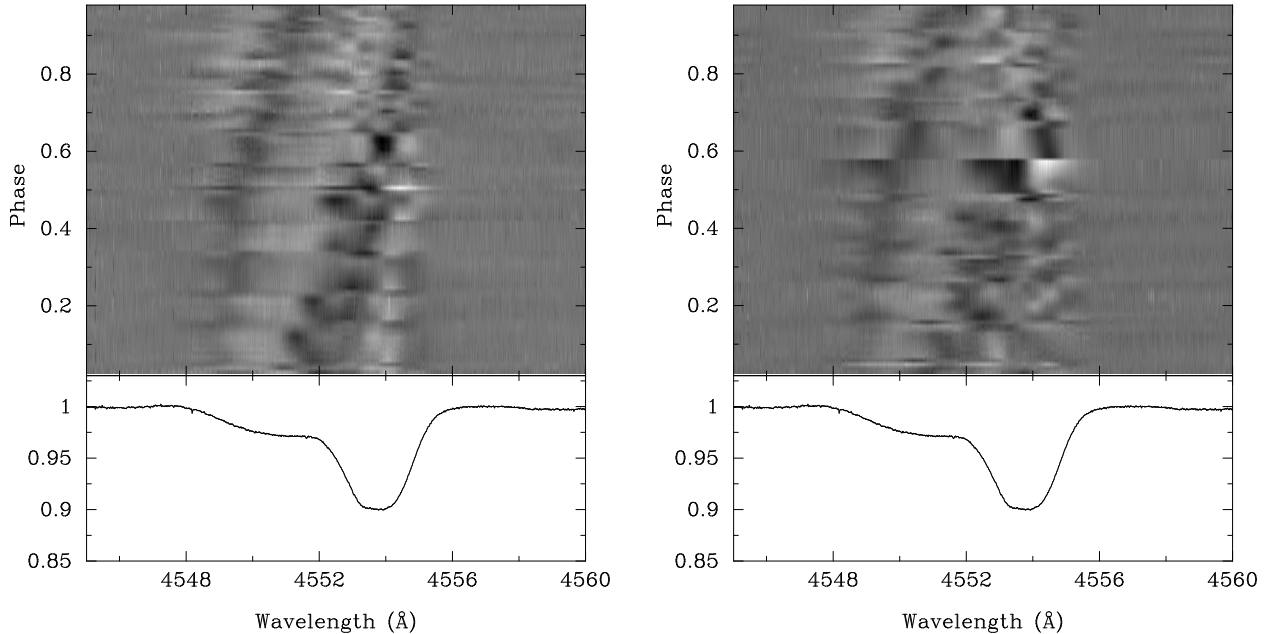


Figure 7. Grey-scale representations of our spectra, phased to the frequencies $f_1 = 5.59$ c/d (left) and $f_2 = 6.28$ c/d (right), with respect to the reference epoch HJD 2447000. The grey-scale shows residuals with respect to the average profile (shown in the lower panels), with black corresponding to local absorption and white indicating local emission.

panel of Fig. 5. Two peaks with an excess power compared to the other peaks occur in the periodogram. Their significance level is similar to that of the 6.37 c/d peak found by Lomb (1975). The two peaks have frequencies $f_1 = 5.59$ c/d and $f_2 = 6.28$ c/d and are about equal in power. Taking into account the results found previously for the star (see Section 3.3), we believe that these two peaks probably represent the true frequencies of radial velocity oscillation.

Phased radial-velocity curves for both frequencies are shown in Fig. 6. A model based on both frequencies accounts for 60% of the variance present in the radial velocity of the stronger line, implying that more modes are present at

lower amplitudes. The high quality of the spectra rules out the remaining variance being due to the noise level of the data. This model gives amplitudes of 2.2 ± 0.4 km s⁻¹ and 2.0 ± 0.4 km s⁻¹ for f_1 and f_2 , respectively, and an average radial velocity for the primary of 63.9 ± 0.3 km s⁻¹.

Figure 7 shows grey-scale representations of our data when folded at f_1 and f_2 (reference epoch HJD 2447000). The figure shows residuals with respect to the average profile. It is clear from these representations that β Cen shows line-profile variability and that the patterns point to a complicated multi-periodic pulsation. The left panel of Figure 7, phased at frequency f_1 , shows a clear progression of line

residuals from blue to red, which is a signature of non-radial pulsations (Yang & Walker 1986). The progression is less clear when the data are phased using f_2 , showing that variations at f_1 dominate.

In the grey-scale representations we also see variability in the spectrum at the wavelength of the secondary’s Si III line. In an attempt to determine whether this effect is due to contamination by the variation of the lines of the primary or to intrinsic variability of the secondary, we found the power spectrum of the velocity variations of the secondary’s line, using its first moment as the velocity indicator. However, due to the greater width of the secondary line, and blending with the primary line, the results are uncertain. The power spectrum shows the same two frequencies f_1 and f_2 . This could be caused either by line blending leading to contamination by the primary’s variation, or, more interestingly, by the secondary exhibiting similar pulsation modes. If this latter speculation is true, Figure 7 suggests that the variations of the secondary may be tidally locked to those of the primary. Finally, we determined the average radial velocity for the secondary to be $-106.3 \pm 0.5 \text{ km s}^{-1}$ at the epoch of our observations (1988 May 16-20).

3.3 Comparison with previous studies

Three previous studies of radial velocity variability in this star have been published. Breger (1967) reported short-term variability with a period of either 0.1317 d (7.59 c/d) or 0.1520 d (6.58 c/d), with the ambiguity being due to 1 c/d aliasing (only one-night runs were obtained). Breger’s suggested frequencies would appear to be aliases of our f_1 .

From a set of 22 spectra taken over four nights in 1967, Shobbrook & Robertson (1968) found the most likely period to be 0.1348 d (7.42 c/d). From a set of 39 spectra taken over two nights in 1969, Lomb (1975) found a period of 0.157 d (6.37 c/d). He interpreted the period found by Shobbrook & Robertson (1968) as a 1 c/d alias. Given the short time spans (and hence, poor frequency resolution) of the observations, the frequency found by Lomb (1975) is consistent with our f_2 .

We conclude that β Cen probably has at least two pulsation frequencies. Both frequencies found in earlier spectroscopic data appear to be simultaneously present in the radial velocity of the star. The beat period amounts to 1.45 days. The quality of the data and the limited time spread are possible reasons why the star was found to be mono-periodic in earlier studies. Another explanation could be that the modes change strength during the orbital motion due to tidal forces. Since the orbital parameters are not known for β Cen, we are not able to check if the dates of the observations obtained by the various authors support such a picture. In order to derive accurate spectroscopic orbital parameters, β Cen has been included in our observational programme of the search for forced oscillations in pulsating stars (see Aerts et al. 1998).

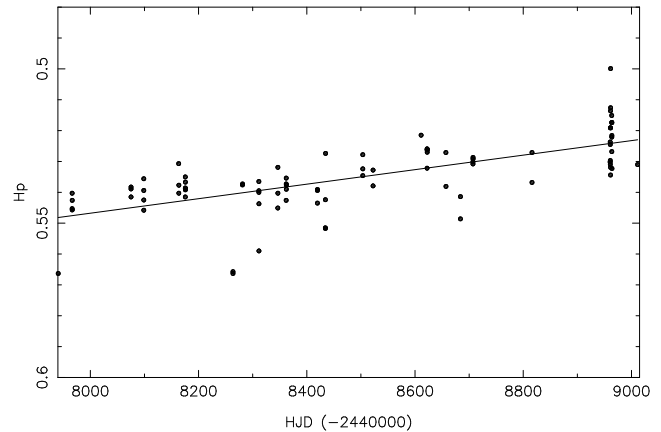


Figure 8. The Hipparcos photometric data (dots) with quality label ≤ 2 for β Cen. The full line represents the least-squares linear fit, which we have subtracted before searching for periodicities in the data

4 HIPPARCOS DATA

β Cen is one of 13 known β Cep stars that are classified as unsolved in the Hipparcos catalogue. This means that the known period of 0.157 d is not recovered in the Hipparcos photometry. This is not surprising, since earlier ground-based photometric surveys have also failed to find a regular variability pattern for this star. The only report of photometric variability is from Strömgren photometry by Balona (1977), who found a 0.30-d periodicity on one night but no variability on a second night. Balona (priv. comm.) observed the star again in 1988 and 1990 and kindly made his data available. We did not find any clear periodicity in these data.

Figure 8 shows the Hipparcos photometry for β Cen, including only those data points having quality label ≤ 2 (for an explanation of the quality labels of the Hipparcos data, see ESA (1997)). There is a clear linear trend, due to instrumental effects, which may have impeded the pipeline analysis. We have therefore re-analysed the Hipparcos photometry by removing the linear trend and looking for periodicity in the residuals by means of the PDM, Scargle, and CLEAN algorithms. We still find no evidence of a clear periodicity, a negative result that is expected for pulsation modes with a relatively high degree ($\ell \geq 3$). Indeed, many of the known β Cep stars for which mode identification has been performed and for which Hipparcos observations also did not recover the periods of variation, do exhibit high degree pulsation. Theoretical instability analyses predict the excitation of modes with degrees up to $\ell = 8$ in β Cep stars (e.g., Moskalik 1995).

5 CONCLUSION

From interferometric measurements using the technique of non-redundant masking, we have shown β Cen to be a close binary. For the epoch 1995 Jan 13 we find the separation to be $15.6 \pm 2 \text{ mas}$ and the position angle to be either $352^\circ \pm 6^\circ$ or $172^\circ \pm 6^\circ$. The parallax of β Cen, as measured by the Hipparcos satellite, is $6.21 \pm 0.56 \text{ milliarcsec}$ (ESA 1997),

which implies that the physical separation of the binary at the epoch of our MAPPIT observations was at least 2.5 AU.

Our spectroscopic measurements reveal β Cen to be double-lined. We detect two pulsation frequencies from radial-velocity variations of the primary star. Further studies of this double star are underway, using both spectroscopy (see Aerts et al. 1998) and also using the Sydney University Stellar Interferometer (J. Davis et al., in prep.). The combined data should allow determination of the orbital parameters and component masses of this system.

ACKNOWLEDGEMENTS

We thank the AAT staff for their help in setting up MAPPIT, and the night assistant Steve Lee. We thank John Davis for suggesting we observe β Cen with MAPPIT and Luis Balona for making available his unpublished time-series photometry. The development of MAPPIT was supported by a grant under the CSIRO Collaborative Program in Information Technology, and by funds from the Australian Research Council. We thank the referee, Chris Haniff, for comments that have improved the paper.

References

- Aerts, C., 1993, PhD thesis, Katholieke Universiteit Leuven, Belgium
- Aerts, C., De Pauw, M., & Waelkens, C., 1992, *A&A*, 266, 294–306
- Aerts, C., De Mey, K., De Cat, P., & Waelkens, C., 1998. In: Bradley, P. A., & Guzik, J. A. (eds.), *A Half Century of Stellar Pulsation Interpretations* Astron. Soc. Pacific Conf. Ser. Vol. 135, 380
- Balona, L. A., 1977, *Mem. R. Astr. Soc.*, 84, 101
- Becker, S. R., & Butler, K., 1990, *A&AS*, 84, 95
- Bedding, T. R., 1992, *MAPPIT: Optical Interferometry with the Anglo-Australian Telescope*, PhD thesis, School of Physics, University of Sydney
- Bedding, T. R., Robertson, J. G., & Marson, R. G., 1994, *A&A*, 290, 340
- Bedding, T. R., Zijlstra, A. A., von der L u e, O., Robertson, J. G., Marson, R. G., Barton, J. R., & Carter, B. S., 1997, *MNRAS*, 286, 957
- Breger, M., 1967, *MNRAS*, 136, 51
- Buscher, D. F., Haniff, C. A., Baldwin, J. E., & Warner, P. J., 1990, *MNRAS*, 245, 7P
- ESA, 1997, *The Hipparcos and Tycho Catalogues*, ESA SP-1200
- Hanbury Brown, R., 1974, *The Intensity Interferometer*, (London: Taylor & Francis)
- Hanbury Brown, R., Davis, J., Allen, L. R., & Rome, J. M., 1967, *MNRAS*, 137, 393
- Hanbury Brown, R., Davis, J., & Allen, L. R., 1974, *MNRAS*, 167, 121
- Haniff, C. A., Mackay, C. D., Titterton, D. J., Sivia, D., Baldwin, J. E., & Warner, P. J., 1987, *Nat*, 328, 694
- Lomb, N. R., 1975, *MNRAS*, 172, 639
- Marson, R. G., 1994. In: Robertson, J. G., & Tango, W. J. (eds.), *IAU Symposium 158: Very High Angular Resolution Imaging*, p. 331, (Dordrecht: Kluwer)
- McAlister, H. A., 1997. In: Bedding, T. R., Booth, A. J., & Davis, J. (eds.), *Proc. IAU Symp. 189, Fundamental Stellar Properties: the Interaction between Observation and Theory*, p. 109 (Dordrecht: Kluwer)
- Moskalik, P., 1995, In: R.S. Stobie, P.A. Whitelock (eds.) *Astrophysical Applications of Stellar Pulsation*, Astron. Soc. Pacific Conf. Ser., Volume 83, p.44.
- Roberts, D. H., Le ar, J., & Dreher, J. W., 1987, *AJ*, 93, 968
- Shobbrook, R. R., 1985, *MNRAS*, 214, 33
- Shobbrook, R. R., & Robertson, J. W., 1968, *Proc. Astron. Soc. Aust.*, 1, 82
- Yang, S., & Walker, A.H., 1986, *PASP*, 98, 1156

This paper has been produced using the Blackwell Scientific Publications L^AT_EX style file.